Cellular ceramics by slip casting of emulsified suspensions

F.R. Cesconeto, J.R. Frade

PII: S0955-2219(20)30257-0

DOI: https://doi.org/10.1016/j.jeurceramsoc.2020.04.002

Reference: JECS 13187

To appear in: *Journal of the European Ceramic Society*

Received Date: 9 December 2019

Revised Date: 31 March 2020

Accepted Date: 1 April 2020

Please cite this article as: Cesconeto FR, Frade JR, Cellular ceramics by slip casting of emulsified suspensions, *Journal of the European Ceramic Society* (2020), doi: https://doi.org/10.1016/j.jeurceramsoc.2020.04.002

Cellular ceramics by slip casting of emulsified suspensions

F.R. Cesconeto[1] and J.R. Frade[1]

[1]CICECO – Aveiro Institute of Materials, Department of Materials and Ceramic Engineering, University of Aveiro, 3810-193 Aveiro, Portugal

Graphical abstracts

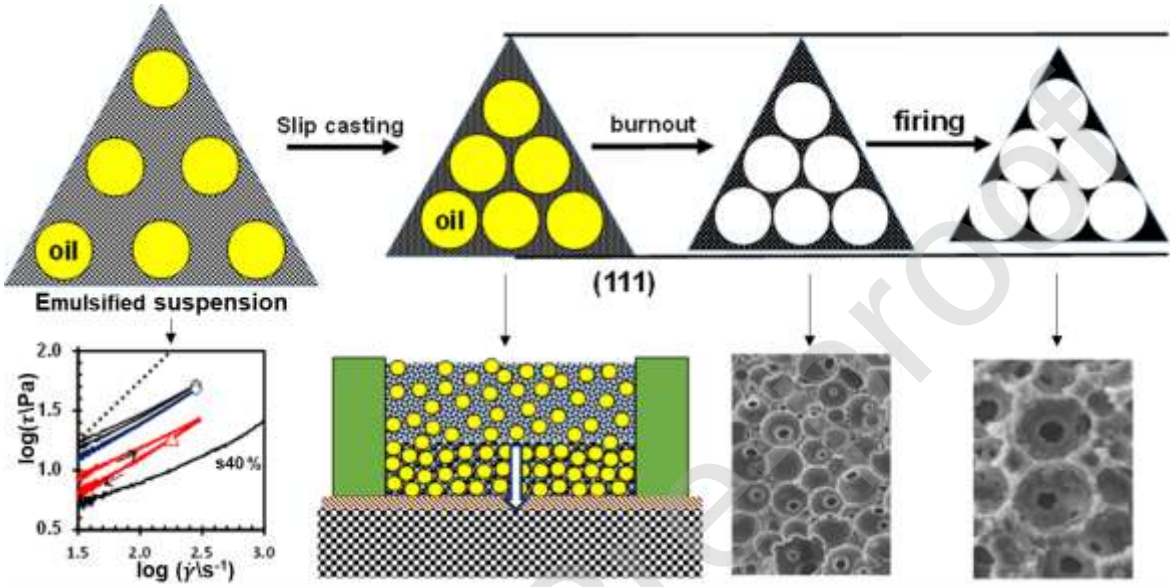

Highlights

- Ceramics with designed cellular microstructures by emulsification of suspensions with edible oil
- Versatile shaping by slip casting
- Ability to minimize undue loss of porosity

ABSTRACT

Cellular ceramics were processed by slip casting of alumina suspensions emulsified with sunflower oil. A model behavior was derived on assuming that the templating dispersed phase and its droplet size distribution are retained as porosity in the resulting cellular ceramics, whereas the continuous ceramic suspension evolves to dense struts and thin inter-pore walls. Representative values of solid load and oil to suspension ratio were selected to seek close packed spatial distribution of nearly spherical. Stirring rate and additions of surfactant were also varied for greater flexibility in adjusting droplet size and rheology of the corresponding emulsified suspensions; this also contributes to minimize undue losses of porosity, relative to the model behavior, and determines microstructural features such as size distributions and average cell size.

Keywords: Cellular ceramics, slip casting, emulsification, colloidal processing

Introduction

Microstructural features of cellular ceramics determine their properties, such as mechanical properties (stiffness, compressive or flexural strength, etc.), percolation for ionic transport or exchange, permeability to fluids, etc... Thus, a variety of methods has been proposed to adjust those microstructural features for the specific requirements of targeted applications, including classical approaches based on impregnation of pore forming scaffolds or dispersion of different pore forming particles in a ceramic matrix. More recently, one finds methods based on emulsification of ceramic suspensions with different organic phases, including volatile alkanes for direct foaming [1] and diverse organic phases as templates for porosity, including higher alkanes [2]. Liquid or melted paraffins [3], and different renewable oils [4] add greater flexibility in processing by de-convolution of steps of drying and subsequent burnout of the organic drops, by analogy with the use of solid sacrificial particles such as PMMA spheres.

Emulsification of ceramic suspensions offers great processing flexibility but requires surfactants to stabilize the emulsified suspensions (e.g. sodium dodecyl sulphate). Alternatively, other additives (e.g. collagen) combine gelcasting and stability for liquid-liquid interfaces, mainly in combination with edible oils as dispersed phase [5]. Pickering emulsification also allows stabilization without surfactants, by adjusting the hydrophilic/hydrophobic behavior of the ceramic particles [6].

Though the main emphasis on processing of cellular ceramics and other highly porous ceramics is microstructural development by different methods of replication, direct foaming or sacrificial templating [7], materials must also be processed with the required shape and within reproducible tolerance. Thus, processing of emulsified suspensions may rely on different casting methods for flexible shaping while preventing collapse of the microstructure during subsequent steps of drying and elimination of the sacrificial phase. Representative examples are gelcasting with collagen [5] and slip casting of Pickering emulsions [8]. The use of non-volatile sacrificial phases also facilitates processing by plastic deformation of emulsified suspensions after partial controlled drying [9]. The present work also demonstrates feasibility of slip casting of suspensions emulsified with sunflower oil and provides guidelines to design the microstructures of resulting cellular ceramics.

Modelling

Fig.1 shows a schematic representation of processing by emulsification of ceramic suspensions and slip casting; this is based on the following assumptions:

i) Emulsification is of oil in water type, with nearly spherical droplets of organic phase dispersed in a ceramic suspension.

ii) Ceramic particles in suspension rearrange to form a packed layer of green ceramic matrix during slip casting, driven by migration of water into the plaster base.

iii) Organic droplets are incorporated in the packed green ceramic layer, maintaining the original organic to solid load ratio in the emulsified suspension, $r_{o:s}{:}\,\phi_s$, and its size distribution, where $r_{o:s}$ denotes the organic to suspension volume ratio and ϕ_s is the solid load in the aqueous suspension.

iv) Subsequent steps of drying do not change the droplet size distribution, and this converts to porosity in the green cellular ceramics, by elimination of the organic phase at intermediate temperatures, while inter-droplet distance narrows to reach close contacts, as depicted in Fig.1.

v) The pore size distribution of the green cellular ceramics is also nearly retained during firing, while strut densify to reach mechanical resistance, and inter-cell walls disrupt at close contacts, giving rise to interconnecting windows, to ensure conditions for percolation or permeability of fluids.

Thus, density of cellular ceramics with close packed porosity, and ideal reproduction of the droplet size distribution, and corresponding solid load to fill dense struts should converge to:

$$x_{id} = \frac{r_{o:s}}{\phi_s + r_{o:s}} \qquad (1)$$

For example, combination of $r_{o:s} = 0.5{:}\,1$ with $\phi_s = 0.45$ yields $x_{id} \approx 0.526$, which is very close to simple cubic packing ($x \approx 0.524$), whereas for $r_{o:s} = 1{:}\,1$ with $\phi_s = 0.45$ yields $x_{id} \approx 0.69$, which is close to body centered cubic (bcc) packing ($x \approx 0.68$), and $r_{o:s} = 1.5{:}\,1$ with $\phi_s = 0.45$ should yield ($x_{id} \approx 0.77$), which is slightly above the face centered cubic (fcc) packing ($x \approx 0.74$). The corresponding values of (oil ratio):(solid load) are $r_{o:s}/\phi_s \approx 2.13$ for ideal bcc packing of nearly spherical droplets, and $r_{o:s}/\phi_s \approx 2.85$ for fcc packing.

Experimental procedure

Cellular alumina ceramics were processed by emulsification of alumina suspensions. A commercial submicrometer alumina powder, d_{50} particle size of 0.5 μm (CT 3000 SG – Alcoa Chemie) was selected to prepare suspensions with 40 or 45 vol%. The suspensions were prepared by milling for 10 min, at 350 rpm, in a planetary ball mill (Retsch PM 100), mixing the alumina powder and deionized water containing 0.5 wt % Dolapix PC 67 (Zschimmer & Schwarz). This deflocculant was added to provide electrostatic stabilization.

These suspensions were emulsified at room temperature, with additions of sodium dodecyl sulphate in powder (SDS) (Sigma-Aldrich) and edible sunflower oil, yielding oil in water emulsification by mechanical stirring with propeller stirrer.

The emulsified suspensions were stirred at 500 or 800 rpm, for 5 minutes, and additions of SDS powder, solubilized directly in the alumina suspension. A critical micellar concentration (CMC) of SDS which is $8.3x10^{-3}$ mol.l^{-1} [10], was used as the basis for this work. It was added in concentrations which correspond to 1, 4 and 9 times the CMC value, i.e., $8.30x10^{-3}$ mol.L^{-1}, $3.32x10^{-2}$ mol.L^{-1} and $7.47x10^{-2}$ mol.L^{-1}, respectively. The oil to suspension volume ratio was $r_{o:s} = 1:1$ or $1.5:1$.

The generic notation of samples is **sl-o-s-rrr** and provides ready information on solid load (sl), oil to suspension ratio (o), surfactant additions (s), and stirring rate in rpm (rrr). For example, 40-1-1-500 was prepared with solid load = 40 vol%, oil: suspension ratio 1:1, with addition of 1 CMC of SDS concentration and stirring at 500 rpm.

A viscometer was used to characterize the rheological behavior of emulsified suspensions with concentric cylindrical geometry as the measuring system (Viscotester IQ, Thermo Haake). The flow curves were performed by changing shear rate between 0 and 300 s^{-1} in two periods, ascending and descending, 60 seconds each, at room temperature.

The emulsified suspensions were slip cast in cylindrical silicone molds on a porous gypsum base at room temperature. The samples were consolidated by extraction of water, driven by capillarity of porous gypsum base, forming a continuous ceramic layer which trapped the organic phase droplets, as depicted in Fig.1. A bottom buffer layer of polypropylene fabric (TNT) was used, between the silicon mold and the gypsum base, to facilitate detachment of the slip casted body after drying. Similarly, a circular polymeric stopper lubricated with detergent soap was used to allow easy side detachment. These slip

casted samples were dried and demolded after 24 h, dried another 2 days still on the gypsum base at room temperature, and then for 2 days at 60 ºC. The organic components were burned out from green bodies by heating at 1 ºC/min up to 200 ºC, then at 5 ºC/min up to 500 ºC, and immediately cooled down to room temperature at -5 ºC/min. These green samples were then analyzed by scanning electron microscopy (SU-70 microscope), after this burnout stage, to characterize the porosity generated by elimination of the dispersed droplets of organic phase. Final firing of cellular ceramics was performed on heating from room temperature up to 1550 ºC, at 5 ºC/min, with a 2h plateau at this temperature and then cooling to room temperature at -5 ºC/min. These fired cellular ceramics were also characterized by SEM combined with stereological analysis, performed with ImageJ software.

Total porosity x_t was measured by the Archimedes method, based on combination of three weight measurements in dry condition wt_1, after impregnation with water wt_2, and with impulsion in water wt_3 [3]:

$$x_t = 1 - \frac{\rho_w}{\rho_{th}} \times \frac{wt_1}{wt_2 - wt_3} \quad (2)$$

where ρ_w is density of water and ρ_{th}=3.99 g·cm^{-3} is the theoretical density of alumina obtained from X-ray diffractograms. Open porosity (x_0) was also calculated as:

$$x_0 = \frac{wt_2 - wt_1}{wt_2 - wt_3} \quad (3)$$

Results and discussion

The graphic of shear stress (τ) vs shear rate ($\dot{\gamma}$), in log-log scales, of suspensions and emulsified suspensions (Fig.2), shows clearly the shear thinning, as revealed by low slope (<1); in the case of emulsified suspension, this resembles a shear thinning often ascribed to onset of flocculation of the dispersed droplets in concentrated oil in water emulsions [11]. Thus, these alternative representations are guideline to analyze fluid shear thinning and to extract the pseudoplastic flow exponent, and relevant parameters which characterize structural changes when a shear stress is applied to a fluid with changes in shear rate between periods ascending and descending, just fitting the Herschel-Bulkley equation. [5]:

$$\tau = \tau_o + k\dot{\gamma}^n \quad (4)$$

where τ and $\dot{\gamma}$ denote shear stress and shear rate, and the fitting parameters τ_o, k and n denote yield stress, consistency coefficient and pseudoplastic flow exponent.

In order to evaluate the different processing conditions over rheological behavior of the emulsified suspensions, firstly, the fitting with the Herschel-Bulkley equation was performed by searching for the value of the pseudoplastic flow coefficient (*n*) which yielded the best correlation between the parameters $\tau\ vs\ \dot{\gamma}^n$. After that the alternative representation was plotted to find the others fitting parameters from the intercept and slope. These parameters are presenting in table 1.

These fitting parameters show more extensive shear thinning for sample 40-1-1-500, as indicated by larger hysteresis, demonstrated by changes in apparent viscosity, pseudoplastic coefficient and yield stress on reverting from increasing shear rate ($\boldsymbol{\eta'_{50}}$, $\boldsymbol{n'}$ and $\boldsymbol{\tau'_o}$) to decreasing shear rate ($\boldsymbol{\eta''_{50}}$, $\boldsymbol{n''}$ and $\boldsymbol{\tau''_o}$).

Those structural changes responsible for shear thinning and hysteresis in sample 40-1-1-500 are, mostly likely, related to conditions of emulsification, with emphasis on low surfactant additions and low stirring rate. However, low stirring rate seems the prevailing factor, since increase in both factors gives higher pseudoplastic coefficient and lower hysteresis in sample 45-1-4-800, whereas significant shear thinning, and hysteresis was retained in sample 45-1.5-9-500 with still higher additions of surfactant.

Structural changes in sample 45-1.5-9-500 might also depend on relatively high solid load and volume fraction of organic phase, with impact on viscosity [11]. Note that solid load is higher than for sample 40-1-1-500, and the fraction of organic phase is higher than 40-1-1-500 and 45-1-4-800, thus explaining differences in viscosity.

The effect of higher solid load in samples 45-1.5-9-500 and 45-1-4-800 is consistent with reported trends for dependence of viscosity on solid load in ceramic suspensions [12], and multiple systems containing a dispersed phase in the ceramic suspensions, namely dispersed polymeric spheres added as pore formers [13] or organic droplets in emulsified suspensions, referred to as suspoemulsions. In this case, the dependence on the fraction of solids has described by a Mooney-type equation [14]:

$$\frac{\eta_{suspoemulsion}}{\eta_{emulsion}} = exp\left(\frac{6.3\phi_s}{1-1.455\phi_s}\right) \quad (5)$$

which predicts an impressive increase in viscosity ratio, by a factor of about 9, on increasing the fraction of solids from 0.40 (in sample 40-1-1-500) to 0.45 (in 45-1-4-800), while keeping a constant content of organic phase. The actual differences between these

samples are much smaller (Table I) and even smaller differences are found between the corresponding suspensions with solid load of 40% (0.114 Pa.s at $\dot{\gamma}$ =50 s^{-1})) and 45 % (0.124 Pa.s). Thus, Eq.4 overestimates the role of solid load. Viscosity of the emulsified suspensions also increases with the volume fraction of dispersed organic phase, mainly for very high fractions of dispersed phase, when droplets are in close contact, possibly interacting and undergoing shape changes, with impact on yield stress and viscosity [15]. In fact, viscosity of sample 45-1.5-9-500 is significantly higher than for the remaining samples (Table I).

Changes in droplet sizes and their distributions may also require optimization for the impact on rheology of the emulsified suspension and because droplet size distributions act as templates for pore size distributions in cellular ceramics processed by emulsification of suspensions and their slip casting. In fact, one assumed that the cell size distribution obtained by stereology of SEM microstructures (Fig.3) can be taken as a guideline for droplet size distributions in the starting emulsified suspensions. This seems a reasonable assumption by considering that pores retain nearly spherical symmetry in green samples of cellular ceramics, after burning out the organic phase and before onset of sintering mechanisms. The final fired samples also retain close similarity with the microstructural characteristics of green samples.

Thus, average cell sizes of cellular ceramics and their size distributions (Table I) were related to processing conditions with emphasis on stirring rate, which determines conditions required to deform and disrupt the droplets, breaking them in smaller sizes (D), combined with other factors with impact on viscosity of the continuous phase η_c, as predicted by their interactions in Reynolds number (Re):

$$Re = \frac{\rho_c\,(0.5D\gamma)D}{\eta_c} \qquad (6)$$

Therefore, droplet sizes in the emulsified suspensions, and corresponding pore sizes in resulting cellular ceramics, should be correlated with conditions of emulsification, namely stirring rate and surfactant additions, possibly combined with the fraction of organic phase. Actually, results in Table I indicate that stirring rate should be the controlling factor, as this yields finer cell sizes in sample 45-1-4-800 by increasing the rate from 500 rpm to 800 rpm, while dropping the additions of surfactant concentration from 9 times de concentration of SDS in sample 45-1.5-9-500 to 4 times in sample 45-1-4-800.

Cell size distributions (Fig.4) provide additional guidelines for correlations between processing conditions and microstructural features of resulting ceramics.

The most obvious difference refers to broader size distribution for sample 40-1-1-500 than for other samples, as illustrated in Fig.4; this is clearly shown by differences in standard deviation, which is much higher than for other samples. The standard deviation to average size is also much higher for sample 40-1-1-500 (7.20). In addition, Fig.4 shows relevant deviations from normal distribution of cell sizes, with significant negative skewness, measure of lack of symmetry in data distribution, for samples 45-1-4-800, and positive skewness for other samples (Table I). Positive skewness observed for samples 40-1-1-500 and 45-1.5-9-500 (Table I) is consistent with low stirring rate at the emulsification stage (500 rpm). Note that SEM microstructures show that most droplets retain nearly spherical shape, without evidence of significant droplet re-coalescence by over-processing during the emulsification stage [16] or arrested coalescence during the slip casting or drying steps; this should yield merging and distorted droplets arrested by partial extraction of water from the surrounding matrix and corresponding viscoelastic changes [17], except possibly by disruption the inter-droplet contacts. Note the interconnecting windows in SEM microstructures (Fig.3), after the burnout stage to eliminate the templating droplets at temperatures below 500 ºC, and well below temperatures onset of sintering mechanisms. Thus, disruption of thin inter-cell walls may occur at an earlier stage before, probably induced by progressive drying at the slip casting and/or drying steps. Thus, one may assume that stirring rate was somewhat insufficient to disrupt relatively large droplets of the discontinuous phase, thus extending the tail of the distribution in the upper range of droplet sizes. Nevertheless, higher additions of surfactants in sample 45-1.5-9-500 are expected to lower the interfacial energy (σ), contributing to overcome the stress (σ/D) required to break large droplet sizes into smaller sizes (D), as observed, and stabilizing the fraction of smaller droplets, as soon as large droplets are divided.

The negative skewness of sample 45-1-4-800 corresponds to sharper decay of the size distribution in the high size tail; this indicates that emulsification in suitable conditions of stirring rate (800 rpm) and surfactant brings the upper limit of the size range closer to conditions when the capillary number ($Ca = 0.5D\eta_c\gamma/\sigma$) approaching its critical value number (Ca_{cr}) [15], and close dependence of droplet size (D) on viscosity of continuous phase (η_c), shear rate (γ) and interfacial energy (σ). Since larger droplets

are more likely to deform and spilt in smaller droplets, this minimizes the upper limit of the size range:

$$D_{max} = \frac{\sigma(1+\delta)\, Ca_{cr,}}{\eta_c \dot{\gamma}} \quad (5)$$

This may explain the narrower size distribution of sample 45-1-4-800.

Porosity of the cellular ceramics obtained by emulsification of ceramic suspensions is predominantly open, with 1-2 % of residual closed porosity; this is consistent with existence of interconnecting windows, induced by disruption of thin films at droplet-droplet contents, and revealed by SEM microstructures (Fig.3). Total porosity is slightly lower than the predicted ideal behavior, indicating significant loss of porosity relative to the volume of oil for samples 40-1-1-500 and 45-1.5-9-500.

Loss of porosity of sample 40-1-1-500 can be explained by structural changes during the initial stages of emulsification and slip casting, as indicated by low yield stress, shear thinning and significant hysteresis of stress vs shear rate. In addition, the wide size distribution may also facilitate structural rearrangements, at later stages of burnout of the organic phase and/or during high temperature firing, as struts densify. On the contrary, the loss of porosity of sample 45-1.5-9-500 may be due to its high oil content, which may corresponds to exceeding the upper limit of ideal packing of spherical pores, i.e., $r_{o:s}/\emptyset_s > 2.85$. Results obtained for sample 45-1-4-800 suggest best agreement when porosity is close to ideal packing for body centered cubic packing (0.68).

Conclusions

Slip casting is a suitable shaping method to process cellular ceramics by emulsification of ceramic suspensions, as an alternative to gel casting. Porosity can be adjusted by suitable combination of oil to suspension ratio and solid load, giving rise to close packing of nearly spherical pores. The continuous ceramic suspensions evolve to dense struts and relatively thin walls, which terminate in interconnecting windows. Close agreement between ideal porosity and experimental results was found for total porosity ≈ 0.69, which is close to bcc packing of spherical pores. Significant loss of porosity occurs when the oil ratio to solid load exceeds conditions for fcc packing $r_{o:s}/\emptyset_s = 2.85$. Losses of porosity were also observed when the emulsified suspensions present unsuitable rheology, namely low yield stress, pronounced shear thinning and hysteresis of shear stress vs shear rate. These rheology characteristics were ascribed to insufficient additions of surfactant and low stirring rate during emulsification, which also give rise to larger

droplet sizes. Low surfactant contents and low stirring rate yield relatively large average droplet size of the discontinuous organic phase and wider size distribution, as revealed by corresponding SEM microstructural features of resulting cellular ceramics.

Declaration of interests

The authors declare that they have no known competing financial interests or personal relationships that could have appeared to influence the work reported in this paper.

ACKNOWLEDGEMENTS

This work was supported by project LEANCOMB (refs. 04/SAICT/2015, PTDC/CTM-ENE/2942/2014) and CICECO-Aveiro Institute of Materials (ref. UID/CTM/50011/2013), financed by COMPETE 2020 Programme and National Funds through the FCT/MEC and when applicable co-financed by FEDER under the PT2020 Partnership Agreement. Additional funding was provided by postdoctoral program abroad CAPES / EDITAL Nº 46/2017.

REFERENCES

[1] S. Barg, C. Soltmann, M. Andrade, D. Koch, G. Grathwohl, Cellular ceramics by direct foaming of emulsified ceramic powder suspensions J. Am. Ceram. Soc., 91 (2008) 2823–2829. https://doi.org/10.1111/j.1551-2916.2008.02553.x.

[2] S. Barg., E.G. Moraes, D. Kock, G. Grathwohl, New Cellular ceramics from high alkane phase emulsified suspensions /HAPES), J. Eur. Ceram., Soc., 29 (2009) 2439-2446. https://doi.org/10.1016/j.jeurceramsoc.2009.02.003.

[3] N. Vitorino, J.C.C. Abrantes, J.R. Frade, Cellular ceramics processed by paraffin emulsified suspensions with collagen consolidation, Mater. Lett., 98 (2013) 120–123. https://doi.org/10.1016/j.matlet.2013.02.020,

[4] N. Nayak, N. Vitorino, J.R. Frade, A.V. Kovalevsky, V.D. Alves, J.G. Crespo, C.A.M. Portugal, Design of alumina monoliths by emulsion-gel casting: understanding the monolith structure from a rheological approach, Materials and Design, 157 (2018) 119-129. https://doi.org/10.1016/j.matdes.2018.07.017.

[5] M.F. Sanches, N. Vitorino, C. Freitas, J.C.C. Abrantes, J.R. Frade, J.B. Rodrigues Neto, D. Hotza, Cellular ceramics by gelatin gelcasting of emulsified suspensions with sunflower oil, J. Eur. Ceram. Soc., 35 (2015) 2577–2585. https://doi.org/10.1016/j.jeurceramsoc.2015.03.008.

[6] I. Akartuna, A.R. Studart, E., Tervoort, L.J. Gauckler, Macroporous Ceramics from particle- stabilized emulsions. Advanced Materials, Adv, Mater., 20 (2008) 4714-4718. https://doi.org/10.1002/adma.200801888.

[7] A.R. Studart, U.T. Gonzenbach, E. Tervoort, L. Gauckler, Processing Routes to Macroporous Ceramics: A Review, J. Amer. Ceram. Soc., 89 (2006) 1771-1789. https://doi.org/10.1111/j.1551-2916.2006.01044.x.

[8] B. Neirinck, J. Fransaer, O. Van Der Biest, J. Vleugels, Production of Porous Materials Through Consolidation of Pickering Emulsions, Adv. Eng. Mat., 9 (2007) 57-59. https://doi.org/10.1002/adem.200600191.

[9] N. Vitorino, C. Freitas, M.J. Ribeiro, J.C.C Abrantes, J.R. Frade, Extrusion of ceramic emulsions: Plastic behavior, Appl. Clay Sci., 101 (2014) 315–319. https://doi.org/10.1016/j.clay.2014.08.021.

[10] A. Cifuentes, J.L. Bernal, J.C. Diez-Masa, Determination of critical micelle concentration values using capillary electrophoresis instrumentation. C. Anal. Chem., 69 (1997) 4271-4274. https://doi.org/10.1021/ac970696n.

[11] R. Pal, Shear viscosity behavior of emulsions of two immiscible liquids, J. Coll. Int. Sci., 225 (2000) 359–366. https://doi.org/10.1006/jcis.2000.6776.

[12] D.J. Kim, H. Kim, J.K. Lee, Dependence of the rheological behaviour of electrostatically stabilized alumina slurries on pH and solid loading. J. Mater. Sci., 33 (1998) 2931-35. https://doi.org/10.1023/A:1004398428917.

[13] S.Z.A. Bukhari, J.H. Ha, J. Lee, I.H. Song, Viscosity study to optimize a slurry of alumina mixed with hollow microspheres, J. Korean Ceram. Soc., 52 (2015) 403-409. https://doi.org/10.4191/kcers.2015.52.6.403.

[14] R. Pal, Rheology of blends of suspensions and emulsions, Ind. Eng. Chem. Res., 38 (1999) 5005-5010. https://doi.org/10.1021/ie990498h.

[15] R. Pal, Rheology of simple and multiple emulsions. Current Opinion, Coll. Int. Sci., 16 (2011) 41-60. https://doi.org/10.1016/j.cocis.2010.10.001.

[16] S.M. Jafari, E. Assadpoor, Y. He, B. Bhandari, Re-coalescence of emulsion droplets during high-energy emulsification, Food Hydrocolloids, 22 (2008) 1191. https://doi.org/10.1016/j.foodhyd.2007.09.006.

[17] C. Hao, Z. Xie, T.J. Atherton, P.T. Spicer, Arrested coalescence of viscoelastic droplets: Ellipsoid shape effects and reorientation, Langmuir, 34 (2018) 12379-12386. https://doi.org/10.1021/acs.langmuir.8b02136.

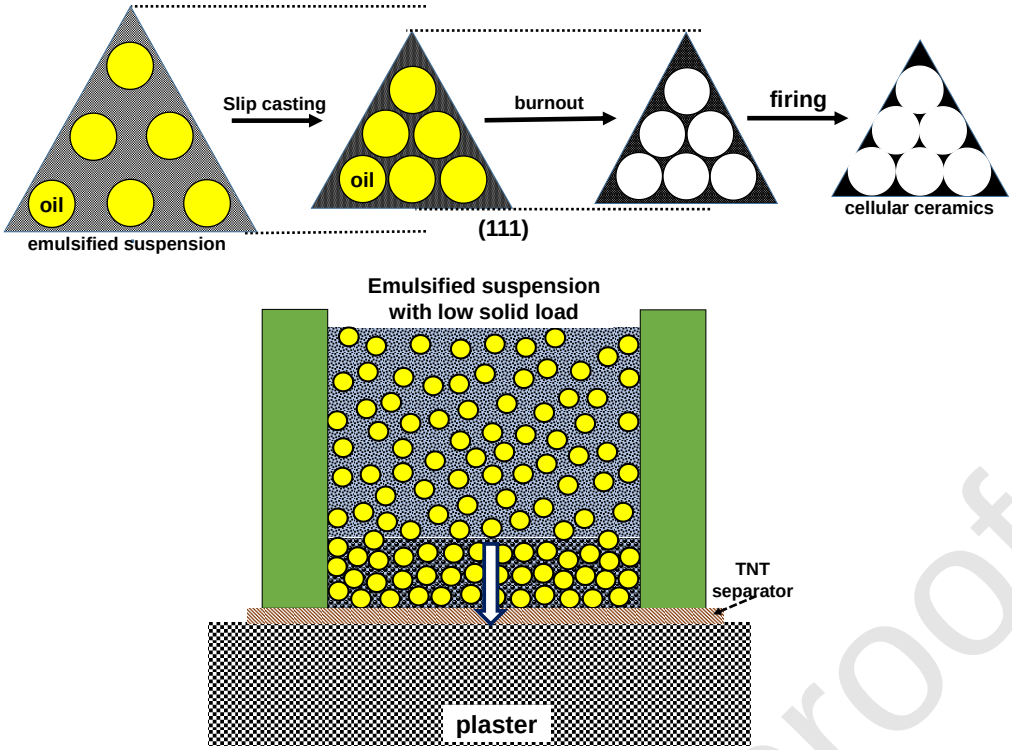

Fig.1 Schematic representation of slip casting of emulsified suspensions.

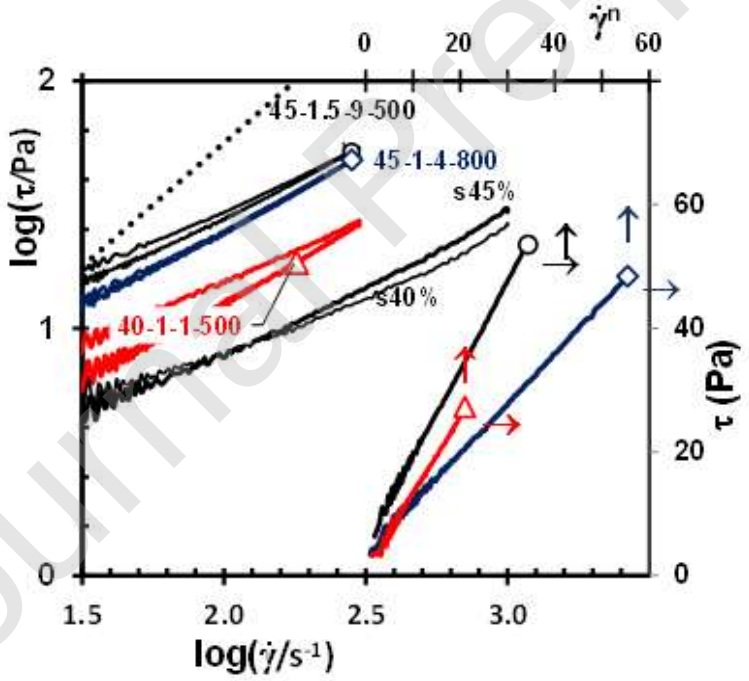

Fig.2: Shear stress vs shear rate in log-log scales obtained for alumina suspensions with 40 vol% and 45 vol% (s40 vol% and s45 vol%) and emulsified suspensions (40-1-1-500, 45-1-4-800 and 45-1.5-9-500). Alternative representations based on Herschel-Bulkley equation are also shown for results obtained with increasing shear rate (secondary axes).

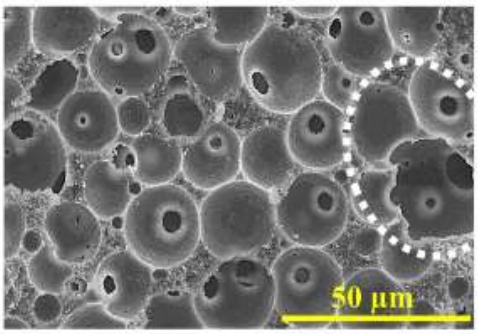

40-1-1-500 (burnout)

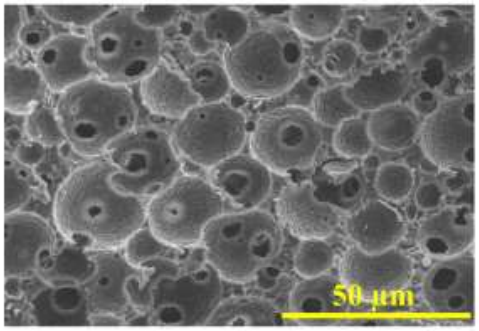

40-1-1-500 (fired)

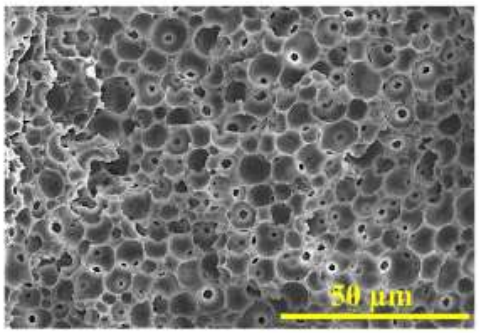

45-1-4-800 (burnout)

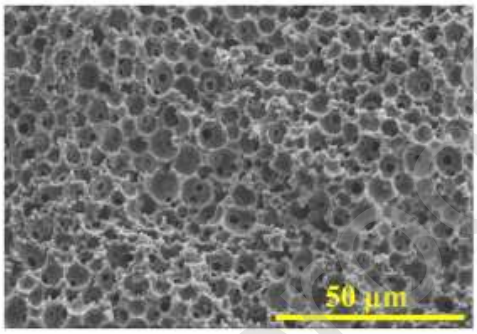

45-1-4-800 (fired)

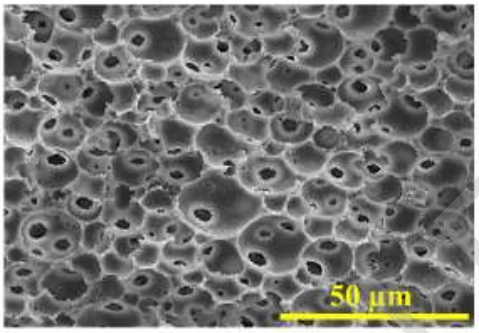

45-1.5-9-500 (burnout)

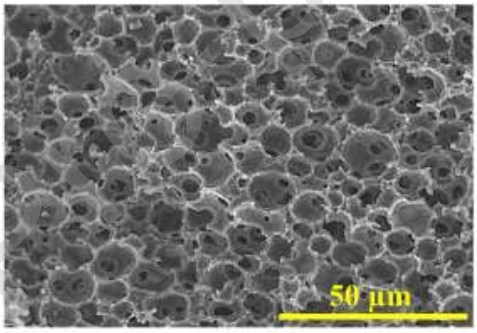

45-1.5-9-500 (fired)

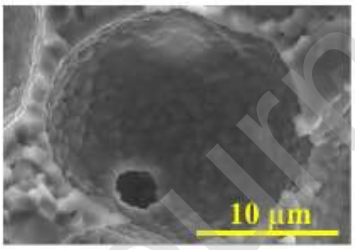

40-1-1-500 (fired)

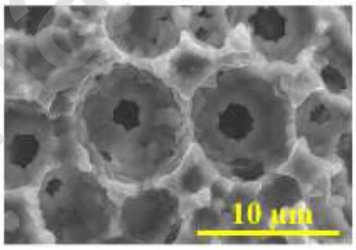

45-1-4-800 (fired)

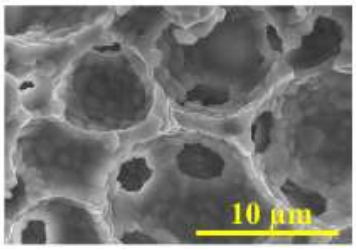

45-1-9-500 (fired)

Fig.3: SEM microstructures of fracture surfaces after burnout of the dispersed organic phase, and after firing (40-1-1-500, 45-1-4-800 and 45-1.5-9-500).

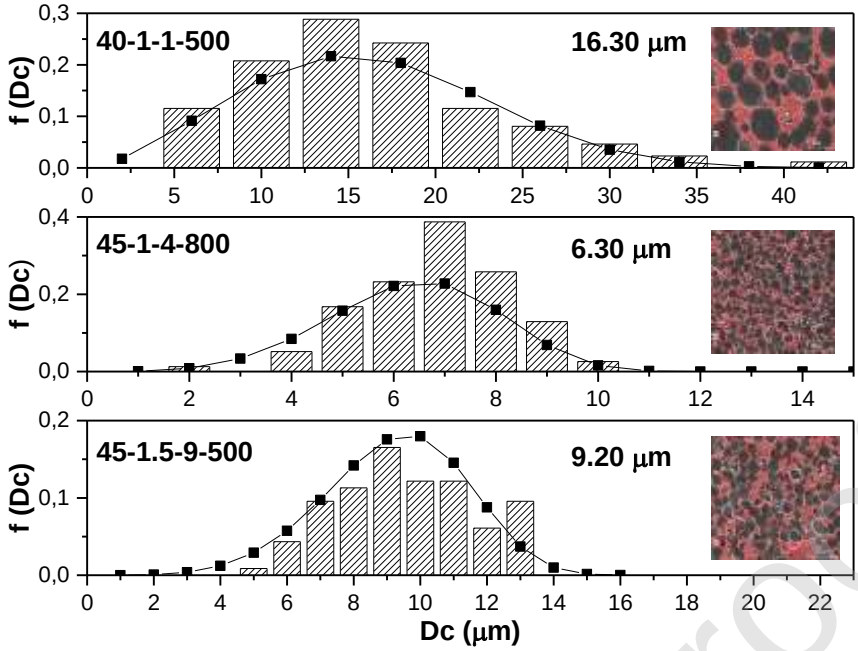

Fig.4: Size distributions of ceramic samples and SEM microstructures of flat surfaces 40-1-1-500, 45-1-4-800 and 45-1.5-9-500.

Fig.5: Compressive strength obtained for cellular ceramic samples 40-1-1-500 (triangles), 45-1-4-800 (circles) and 45-1.5-9-500 (squares).

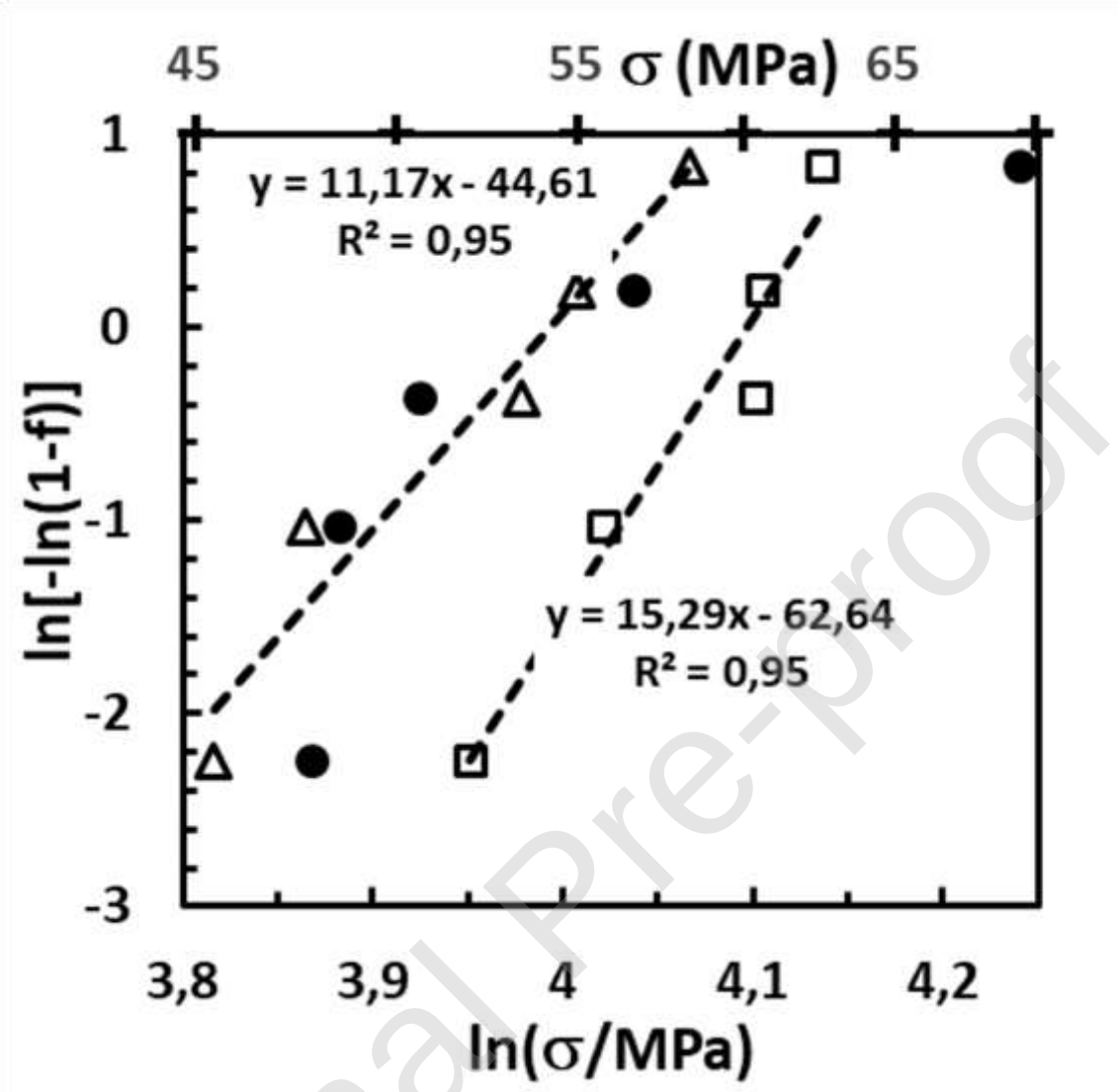

Table I: Experimental conditions, corresponding impact on rheology parameters of the emulsified suspensions, porosity (x %) and its ideal value given by Eq.1, and microstructural characteristics of resulting cellular ceramics obtained by slip casting (average cell size D_c, standard deviation s.d, and skewness). The prime superscript denotes parameters extracted from data obtained with increasing shear rate and double prime corresponds to decreasing shear rate.

		40-1-1-500	45-1-4-800	45-1.5-9-500
Processing	ϕ_s	0.40	0.45	0.45
	$r_{o:s}$	1:1	1:1	1.5:1
	[SDS]	1	4	9
	rate (rpm)	500	800	500
Rheological parameters	η'_{50} **(Pa.s)**	0.22	0.34	0.43
	η''_{50} **(Pa.s)**	0.16	0.32	0.38
	τ'_o **(Pa)**	0.51	3.50	4.25
	τ''_o**(Pa)**	1.71	3.40	5.10
	n'	0.53	0.71	0.62
	n''	0.74	0.73	0.70
	k' **(Pa.s^n)**	0.70	0.81	1.46
	k'' **(Pa.s^n)**	1.30	0.81	1.48
Cellular Ceramics	**x (%)**	63 %	67 %	68 %
	x_{id} **(%)**	71 %	69 %	77 %
	$(x_{id} - x)$	8.5 %	2.0 %	9.0 %
	D_c (µm)	16.30	6.30	9.20
	s.d. (µm)	7.12	1.50	2.10
	Skewness	0.78	-0.38	0.16